DTU Library

Multipurpose FCS Model Predictive Control of VSC-Based Microgrids for Islanded and Grid-Connected Operation Modes

Ghiasi, Mohammad; Niknam, Taher; Dehghani, Moslem; Baghaee, Hamid Reza; Wang, Zhanle; Ghanbarian, Mohammad Mehdi; Blaabjerg, Frede; Dragicevic, Tomislav

Published in:
IEEE Systems Journal

Link to article, DOI:
10.1109/JSYST.2022.3215437

Publication date:
2023

Document Version
Peer reviewed version

Multipurpose FCS Model Predictive Control of VSC-Based Microgrids for Islanded and Grid-Connected Operation Modes

Mohammad Ghiasi, *Member, IEEE*, Taher Niknam, *Senior Member, IEEE*, Moslem Dehghani, Hamid Reza Baghaee, *Member, IEEE*, Zhanle Wang, *Member, IEEE*, Mohammad Mehdi Ghanbarian, Frede Blaabjerg, *Fellow, IEEE*, and Tomislav Dragicevic, *Senior Member, IEEE*

***Abstract*—This article presents an enhanced control strategy for renewable energy resources connected to the grid through voltage-sourced converters (VSCs) in microgrids. The proposed scheme contains a voltage control loop with the minimum inverter switching, a power-sharing controller with the minimum inverter switching, a negative-sequence current controller, and a loop to identify the control system operation mode. All the controllers are designed using the multipurpose finite control set-model predictive control (FCS-MPC) strategy. Since these controllers use the dynamic current and VSC voltage, they can be applied in grid-connected and island operation modes and transferred between them. The method uses voltage–frequency control instead of power control for VSCs. One inverter controls voltage, and the other controls current. The conventional FCS-MPC is enhanced to reduce the computation power by eightfold. This improvement is significant because the maximum switching frequency is limited in practical implementations. Also, the superiority of the proposed multipurpose control scheme is proved theoretically. Simulation is implemented using MATLAB software and compared with methods in the literature. The simulation demonstrates that the presented control strategy is efficient, authentic, and compatible. The proposed method is also tested and validated in hardware experiments.**

***Index Terms*—Current controller, finite control set-model predictive control (FCS-MPC), grid-connected operation mode (GCOM), islanded operation mode, voltage controller.**

I. Introduction

MICROGRID (MG) is a small-scale low-voltage power grid that can improve both energy efficiency and local system flexibility [1]. MGs generally contain many distributed generation (DG) units, and those DGs are typically connected to the MGs via power electronic converters/inverters. Since MGs are able to operate in grid-connected or island mode, the converters/inverters controls are designed to enable the two-mode operation [2], [3]. To improve the system's stability, DGs in MG can operate in island mode in the event of a power outage from the main grid. Therefore, they can keep the load's voltage and frequency in the normal range [4]. The continuous operation of DGs has several benefits, including improving network reliability and additional revenue generation [5]. To properly operate DG units in the island mode, the system needs special control schemes [6]. The main utility dictates the voltage/frequency of the grid-connected mode according to an external control reference. Also, DGs can provide active power (P) and reactive power (Q) in MG. In the island operation mode (IOM) and when there is no communication and power supply to the main network, DGs should supply part or all of loads of the MG [7]. Under such situations, the control systems act as grid-forming controllers. In this regard, a droop control strategy can be utilized for a system with multiple DGs [8]. Generally, the control of frequency, voltage, current, and protection in an island mode is more complicated than in a connected mode. The control issues related to the protection and stability of MGs are somewhat different from conventional power systems. So, paying attention to this topic can open new perspectives for researchers in this field. In MGs, two forms of power sources are utilized: 1) rotating-machine-based sources; and 2) converter-interfaced sources. Combining different energy sources can cause various challenges in grid control during both operation modes. Converters, as fast sources, can respond quickly to power system disturbances [9]. Since system dynamics are much slower with rotating-machine-based sources, coordinating these sources can create new challenges. Another challenge of MGs is the

Manuscript received 16 February 2022; revised 4 July 2022 and 15 September 2022; accepted 9 October 2022. *(Corresponding authors: Taher Niknam; Hamid Reza Baghaee.)*

Mohammad Ghiasi is with the Department of Electrical and Electronics Engineering, Shiraz University of Technology, Shiraz 7155313, Iran, and also with the Faculty of Engineering and Applied Sciences, University of Regina, Regina, SK S4S 0A2, Canada (e-mail: mgy918@uregina.ca).

Taher Niknam and Moslem Dehghani are with the Department of Electrical and Electronics Engineering, Shiraz University of Technology, Shiraz 7155313, Iran (e-mail: niknam@sutech.ac.ir; mo.dehghani@sutech.ac.ir).

Zhanle Wang is with the Faculty of Engineering and Applied Sciences, University of Regina, Regina, SK S4S 0A2, Canada (e-mail: zhanle.wang@uregina.ca).

Hamid Reza Baghaee is with the Department of Electrical Engineering, Amirkabir University of Technology, 159163-4311 Tehran, Iran (e-mail: hrbaghaee@aut.ac.ir).

Mohammad Mehdi Ghanbarian is with the Department of Electrical Engineering, Kazerun Branch, Islamic Azad University, Kazerun MJ42+5V2, Iran (e-mail: mghanbarian.kau@gmail.com).

Frede Blaabjerg is with the Department of Energy Technology Power Electronic Systems, Faculty of Engineering and Science, Aalborg University, 9220 Aalborg, Denmark (e-mail: fbl@et.aau.dk).

Tomislav Dragicevic is with the Center for Electrical Power and Energy, Department of Electrical Engineering, Technical University of Denmark, 2800 Copenhagen, Denmark (e-mail: tomdr@elektro.dtu.dk).

Digital Object Identifier 10.1109/JSYST.2022.3215437

stabilization of operation from grid-connected to island mode transmission. Therefore, an appropriate control strategy should be adopted for fast and correct transmission (from grid-connected to IOM), which also leads to network stability [10]. Various techniques, such as deadbeat control [11], adaptive control [12], and multiloop feedback control [13], have been widely used in MGs. Model predictive control (MPC) has been widely used in MGs to control and stabilize power systems among different control systems. For example, in [14], the controller robustness versus grid disturbances was investigated. In [15], an MPC strategy was proposed based on applying a dynamic output *LC* filter of the inverter for a uninterruptible power supply (UPS). Also, Jafari et al. [16] addressed a general adaptive control layout that includes an external power loop and an inner voltage and current loop to adjust the output voltage and the inverter load flow. In [17], the MPC applications in the parallel-connected inverters control were discussed. The main focus was on the inverter control for a UPS in the standalone operation with different approaches. A simple MPC-based control layout was proposed, which does not need modulators or internal current control loops [18]. Enhanced MPC methods can also be seen in the literature. For example, Mayer et al. [19] proposed an MPC scheme in a unit commitment problem to minimize the generation cost while meeting a nonlinear load. A load frequency control method was proposed in [20] by applying a distributed MPC method for a multiarea intercoupled electrical network. A discrete model of inverters was presented in [21] for two kinds of pulse width modulation (PWM), which are exactly assigned to the voltage pattern. Besides, MPC is desirable for power converter control due to its flexibility, constant converter operation, and efficient current tracking. It can also overcome limitations, such as system nonlinearity, duty cycle saturation, and maximum acceptable current [22]. More specifically, the MPC method predicts the system behavior utilizing the control action and the present modes. Afterward, a cost function is used in the role of a standard to select the optimal switching modes [15].

The MPC control methods can be found in many applications, such as controlling reactive and active powers of rectifiers [23], electromagnetic torque of electric drives [24], and the current or voltage of inverters systems. In [25], MPC was developed to reduce reactive and active powers ripple of nonislanding inverters in a PV network. In addition, a pattern-based prediction layout was implemented to make up for a one-step delay. Also, a two-step horizon prediction technique was proposed to reduce inverter switching loss. In [26], an MPC strategy for an inverter was proposed in a renewable power generation system to achieve grid synchronization, grid-connected operation mode (GCOM), and IOM. Using different cost functions, this control strategy can achieve constant voltage, smooth and quick grid synchronization, and pliable reactive and active powers regulation.

MPC methods for power electronic control can be generally arranged into two different classes: 1) continuous control set-MPC (CCS-MPC); and 2) finite-control set-model predictive control (FCS-MPC) [22]. CCS-MPC can be found in many applications, such as flying capacitor converters, three-level neutral point clamped, matrix converters, and cascaded h-bridge multilevel converters [26].

MPC application in power electronic converters has appropriate performances, such as decreasing the frequency of switching, bettering load transients, balancing the voltage of the load, reducing the loss of communication, and diminishing the total harmonic distortion (THD) [27]. This procedure is easy and does not need modulation. Zaouche et al. [28] used the FCS-MPC in the high-power medium voltage (MV) wind energy conversion systems. The proposed method controlled the turbine's reactive and active powers and the dc-link capacitor voltages. Also, in [29], an FCS-MPC design was presented for PWM modulation and cascade control loops.

This work proposes a multipurpose FCS-MPC (MFCS-MPC) scheme that contains a voltage control loop with the minimum inverter switching, a power-sharing control loop with the minimum inverter switching, a negative-sequence current controller, and a loop to identify the operation mode of the control system. In contrast with other conventional FCS-MPC techniques, the measured reactive and active powers are used in the proposed methodology. The presented control strategy can compensate for harmonics and unsymmetric currents. Remarkably, this scheme has less complexity than prior methods. In this article, we present theoretical and methodical ideas and concepts, provisions, and essential conditions to have a robust and stable performance in the proposed MFCS-MPC strategy in both IOM and GCOM. The simulation in MATLAB/Simulink demonstrates that the proposed strategy is efficient, authentic, and compatible. The simulation results are compared with other reported MPC techniques in different load kinds, such as linear symmetric, nonsymmetric, and nonlinear loads. Finally, we validated the proposed approach and simulation in hardware experiments using realistic assumptions and considerations. The main contributions of this research work are summarized as follows.

1) The conventional FCS-MPC is enhanced, and the computational time is reduced eightfold.
2) The proposed method's switching frequency is relatively low, which is important since the maximum switching frequency is limited in practical implementations.
3) The steady-state measures, such as output voltage peak, output voltage effective value, and THD, have been improved in comparison to MPC and proportional-integral (PI) controllers.
4) Power quality is improved in both symmetric and unsymmetric loads.

The rest of this article is organized as follows. Section II elaborates on the system description and modeling. Section III outlines the proposed MFCS-MPC controller design procedure for both IOM and GCOM, and voltage and power flow controllers are designed. Offline digital time-domain simulation results for various scenarios in GCOM and IOM, along with comparisons with other reported MPC techniques, are given in Section IV. In Section V, the results of the experimental test are provided. Finally, Section VI concludes this article.

II. System Modeling

MG can operate in GCOM or IOM. In the GCOM, the utility grid controls frequency and voltage, and the MG controls the current. Three DG units are controlled to provide demanded

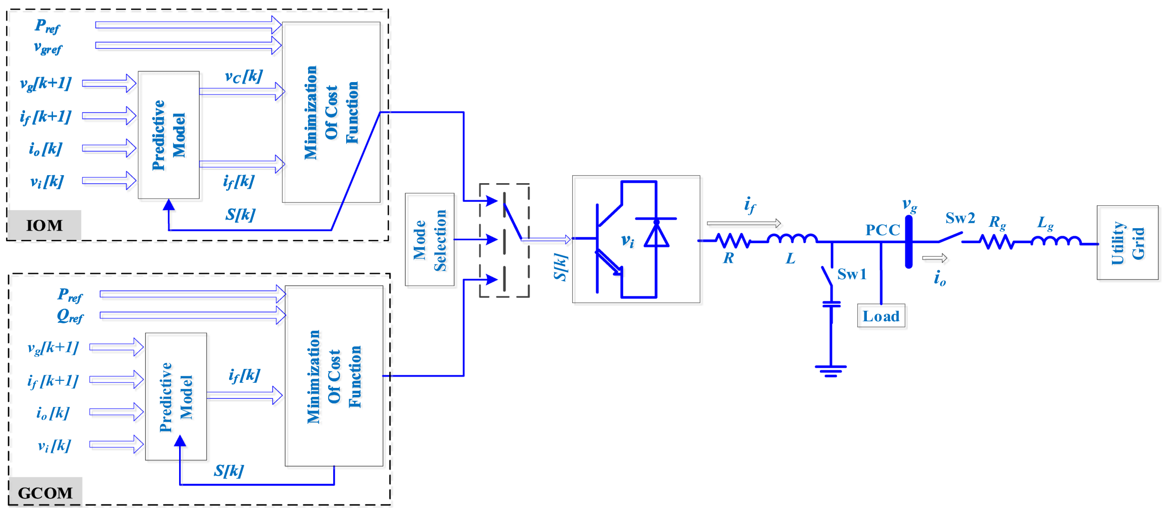

Fig. 1. Controller layout and circuit diagram for the three-phase grid-connected inverter.

power and compensate for the power quality. Each DG unit composes *LC* filters, a dc source, and a voltage-sourced converter. In the GCOM, if the utility grid is strong, the MG voltage will be controlled by the utility grid. In addition, the *L*-type filter will suppress the inverter output harmonic, and the capacitor will be disconnected. However, the MG will control the voltage if the grid is weak or the grid voltage drops. In IOM, the MG solely supplies the demanded power in a predefined power-sharing scheme and controls the load voltages and frequency. In this mode, the *LC*-type filter suppresses the inverter output harmonics. The power circuit and schematic control diagram of a three-phase inverter by an *LC* filter in IOM are shown in Fig. 1. The three-phase inverter is modeled as

$$L\frac{\mathrm{d}}{\mathrm{d}t}\left(i_f^J\right) = S_J\, V_{\mathrm{dc}} - v_{gJn};\; J = a, b, c \tag{1}$$

where

$$S_a = \begin{cases} 1 & \text{if } S_1 = \text{ON} \quad S_4 = \text{OFF} \\ 0 & \text{if } S_1 = \text{OFF} \quad S_4 = \text{ON} \end{cases}$$

$$S_b = \begin{cases} 1 & \text{if } S_2 = \text{ON} \quad S_5 = \text{OFF} \\ 0 & \text{if } S_2 = \text{OFF} \quad S_5 = \text{ON} \end{cases}$$

$$S_c = \begin{cases} 1 & \text{if } S_3 = \text{ON} \quad S_6 = \text{OFF} \\ 0 & \text{if } S_3 = \text{OFF} \quad S_6 = \text{ON} \end{cases} \tag{2}$$

where V_{dc} defines the dc-link voltage, a, b, and c are our three phases, v_{gan}, v_{gbn}, and v_{gcn} denote the phases to neutral voltages after filtering, and i_f^a, i_f^b, and i_f^c represent the currents of phases by filter inductor *L*. As can be seen, the inverter output voltage vector is shown in Fig. 1, which is expressed as follows:

$$v_i = \frac{2}{3}\left(v_{an} + av_{bn} + a^2 v_{cn}\right) \tag{3}$$

where $a = e^{j2\pi/3}$. There are eight switching modes that considered all the combinations of the gating signals S_a, S_b, and

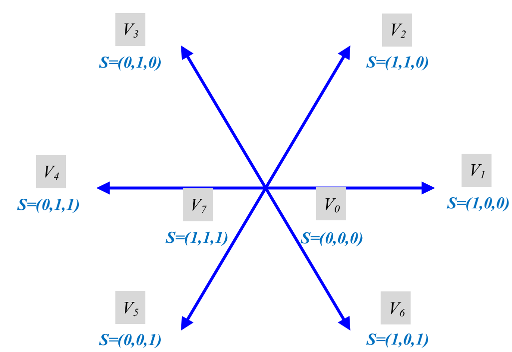

Fig. 2. Inverter output voltage space vectors and switching states.

S_c. Therefore, eight voltage vectors are gained. As $v_0 = v_7$, there are seven voltage vectors, and shown in Fig. 2. Using the Kirchhoff's voltage's law, we have

$$Ri_f^J + L\frac{\mathrm{d}i_f^J}{\mathrm{d}t} = v_i^J(t) - v_g^J(t);\; J = a, b, c. \tag{4}$$

Also, we need to know the Kirchhoff's current law in our circuit, which states that

$$C\frac{\mathrm{d}v_g^J}{\mathrm{d}t} = i_f^J - i_o^J = i_c^J;\; J = a, b, c. \tag{5}$$

State-space representation of each phase is given as

$$\begin{cases} \dot{x}_J(t) = & Ax_J(t) + Bv_i^J(t) + \Gamma i_o^J(t) \\ & y_J(t) = C_J\, x_J(t) \end{cases} \;;\; J = a, b, c \tag{6}$$

where $x_J(t) = \begin{bmatrix} i_f^J(t) \\ v_g^J(t) \end{bmatrix}$ is the state vector and $v_i^J(t)$ denotes the control command and specifies as $\begin{bmatrix} v_1^J(t) \\ v_2^J(t) \end{bmatrix} = \begin{bmatrix} \beta_j\cos(\theta_j)\cos(\omega t) \\ \beta_j\sin(\theta_j)\sin(\omega t) \end{bmatrix}$; also, β_j is a multiple of input voltage value V_{dc}, hence β_j is between zero and one ($0 \le \beta_j \le 1$). $i_o^J(t)$ is the disturbance input. C_J is as $C_J = [1,\ 0]$ for current control, and also it specifies as $C_J = [0,\ 1]$ to control voltage.

$$A = \begin{bmatrix} -\frac{R}{L} & -\frac{1}{L} \\ \frac{1}{C} & 0 \end{bmatrix}, B = \begin{bmatrix} \frac{1}{L} \\ 0 \end{bmatrix}, \Gamma = \begin{bmatrix} 0 \\ \frac{1}{C} \end{bmatrix}$$

$$\begin{bmatrix} v_1^J(t) \\ v_2^J(t) \end{bmatrix} = \begin{bmatrix} \beta_j \cos(\theta_j)\cos(\omega t) \\ \beta_j \sin(\theta_j)\sin(\omega t) \end{bmatrix}, 0 \le \beta_j \le 1. \tag{7}$$

Equation (6) can be discretized to be applied in the controller design as follows:

$$\begin{cases} x_J^D[k+1] = A_D\, x_J^D[k] + B_D v_i[k] + \Gamma_D i_o[k] \\ y_J^D[k] = C_J x_J^D[k] \end{cases}$$
$$J = a, b, c \tag{8}$$

where $x_J^D\ [k] = \begin{bmatrix} i_f^J[k] \\ v_g^J[k] \end{bmatrix},\ A_D = e^{AT_s},\ B_D = \int_0^{T_s} e^{A\tau} B \mathrm{d}\tau$, $\Gamma_D = \int_0^{T_s} e^{A\tau}\Gamma \mathrm{d}\tau$, and T_s is the sampling period.

III. Controller Design

The proposed control scheme contains the following items.

1) Voltage and sharing power control loops with the minimum switching converters.
2) A negative-sequence current control loop.
3) A control system mode detection loop.

The voltage controller keeps the MG bus voltage within acceptable limits. When the loads are unbalanced, the power components oscillate. Here, the negative-sequence current controller is applied to share the current. In this way, the unbalanced load does not impact the grid. Notably, each DG can compensate for its local oscillating power dramatically. Oscillating power components of nonlocal loads are shared between DGs. So, the suggested guideline controller amends the total power quality of the MG. The following section describes the presented controller.

A. Finite-Control Set-MPC

In the MPC algorithm, system modes are predicted along with future time steps $[k, k+n]$, where $n = 1, \ldots, N_p$ and N_p is the prediction horizon. Model of the system and its measured or observed states at time instant k are used to calculate optimal control action minimizing a cost function along with future time steps $[k, k+N_c]$, where $N_c < N_p$ and N_c is the control horizon. Afterward, only the primary calculated control action is used in the system. The procedure is repeated at time step $k+1$. This type of MPC technique is named receding horizon MPC.

The MPC predicts the system behavior only for a limited number of feasible switching modes. The prediction is then utilized to select a switching mode to minimize a cost function. This algorithm is prosperously used for many drive applications and power converters.

B. Problem Formulation

In the following equations, $j = a, b, c$. By applying (8) at $k+1$, then the system output has been estimated as follows:

$$y_J[k+1] = C_J\, A_D x_J^D[k] + C_J B_D v_i[k] + C_J \Gamma_D i_o[k]. \tag{9}$$

The control variation is defined as

$$v_i[k] = v_i[k-1] + \Delta v_i[k]. \tag{10}$$

Then, by using (10) in (9), it gives

$$\begin{aligned} y_J[k+1] = C_J\, A_D x_J^D[k] + C_J B_D v_i[k-1] \\ + C_J \Gamma_D i_o[k] + C_J B_D \Delta v_i[k]. \end{aligned} \tag{11}$$

The system's predicted output parameters have been computed successively with the predicted horizon applying the group of future control variables as

$$\begin{bmatrix} y_j[k+1|\,k] \\ y_j[k+2|\,k] \\ \vdots \\ y_j[k+N_p|\,k] \end{bmatrix} = f_j + S_{fj}\Delta v_{fj} \tag{12}$$

where $S_{lj} = \sum_{i=1}^{l} C_j A_j^{i-1} B_D,\ S_l^d = \sum_{i=1}^{l} C_j A_j^{i-1}\Gamma_D$, and forced response $(S_{fj}\Delta v_{fj})$ and unforced response (f_j) have been retreived as

$$S_{fj} = \begin{bmatrix} S_{(1)j} & 0 & \cdots & 0 \\ S_{(2)j} & S_{(1)j} & \cdots & 0 \\ \vdots & \vdots & \ddots & \vdots \\ S_{(N_p)j} & S_{(N_p-1)j} & \cdots & S_{(N_p-N_c+1)j} \end{bmatrix} \tag{13}$$

$$\Delta v_{fj} = \begin{bmatrix} \Delta v_j[k] \\ \Delta v_j[k+1] \\ \vdots \\ \Delta v_j[k+N_c-1] \end{bmatrix}$$

$$\begin{aligned} f_j = \begin{bmatrix} C_J A_D \\ C_J A_D^2 \\ \vdots \\ C_J A_D^{N_p} \end{bmatrix} x_j[k][k] + \begin{bmatrix} S_{(1)j} \\ S_{(2)j} \\ \vdots \\ S_{(N_p)j} \end{bmatrix} v_{fj}[k-1] \\ + \begin{bmatrix} S_{(1)j}^d \\ S_{(2)j}^d \\ \vdots \\ S_{(N_p)j}^d \end{bmatrix} i_{oj}[k][k]. \end{aligned} \tag{14}$$

The cost function (J), which is reflected the control objective, has been specified as follows:

$$\begin{aligned} \min_{\Delta v_{fa},\, \Delta v_{f_b}, \Delta v_{f_b}} J = \sum_j \sum_{i=1}^{N_p} (r_j[k+i|k] - y_j[k+i|k])^T \\ \times (r_j[k+i|k] - y_j[k+i|k]). \end{aligned} \tag{15}$$

That is regarded to minimize the errors among the predicted output and reference value.

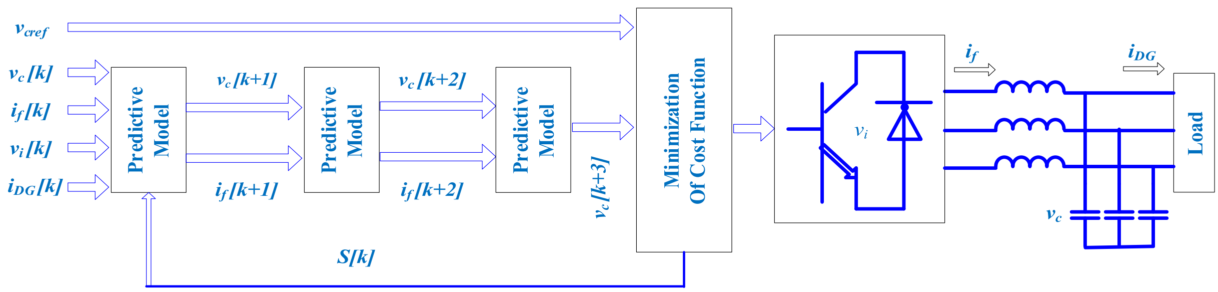

Fig. 3. Block schematic of MPC in IOM.

By choosing the term $r_j - f_j - S_{fj}\Delta v_{fj} = \widehat{\Lambda}$, then (15) is obtained as

$$\min_{\Delta v_{fa},\, \Delta v_{f_b}, \Delta v_{f_b}} J = \sum_j \left(\widehat{\Lambda}_J^T W_j^Y \widehat{\Lambda}_J\right). \tag{16}$$

Suppose that $\Lambda_J = r_j - f_j$, then (16) has been retrived as

$$\min_{\Delta v_{fa},\, \Delta v_{f_b}, \Delta v_{f_b}} J = \sum_j \left(\Lambda_J^T \Lambda_J + \Delta v_{fj}^T \left(S_{fj}^T S_{fj}\right) \Delta v_{fj} - 2\Delta v_{fj}^T S_{fj}^T \Lambda_J\right). \tag{17}$$

Based on (7), the following constrains are retrieved:

$$\mathrm{Max}\,(v_j\,[k-1]) = \begin{bmatrix} \mathrm{Max}\,(\cos(\theta_j)\cos(\omega\,[k-1]\,T_s)\,,0) \\ \mathrm{Max}\,(\sin(\theta_j)\sin(\omega\,[k-1]\,T_s)\,,0) \end{bmatrix} \text{ and}$$

$$\mathrm{Min}\,(v_j\,[k-1]) = \begin{bmatrix} \mathrm{Min}\,(\cos(\theta_j)\cos(\omega\,[k-1]\,T_s)\,,0) \\ \mathrm{Min}\,(\sin(\theta_j)\sin(\omega\,[k-1]\,T_s)\,,0) \end{bmatrix}. \tag{18}$$

By applying constrains in (18) to the optimization problem in (17), we have

$$\begin{bmatrix} I & 0 & \cdots & 0 \\ I & I & \cdots & 0 \\ \vdots & \vdots & \ddots & 0 \\ I & I & \cdots & I \end{bmatrix} \Delta v_{fj} \geq \begin{bmatrix} \mathrm{Min}\,(v_j\,[k-1]) - v_j\,[k-1] \\ \mathrm{Min}\,(v_j\,[k-1]) - v_j\,[k-1] \\ \vdots \\ \mathrm{Min}\,(v_j\,[k-1]) - v_j\,[k-1] \end{bmatrix} \tag{19}$$

$$-\begin{bmatrix} I & 0 & \cdots & 0 \\ I & I & \cdots & 0 \\ \vdots & \vdots & \ddots & 0 \\ I & I & \cdots & I \end{bmatrix} \Delta v_{fj} \geq \begin{bmatrix} v_j\,[k-1] - \mathrm{Max}\,(v_j\,[k-1]) \\ v_j\,[k-1] - \mathrm{Max}\,(v_j\,[k-1]) \\ \vdots \\ v_j\,[k-1] - \mathrm{Max}\,(v_j\,[k-1]) \end{bmatrix}. \tag{20}$$

Finally, the following constrained MPC is achieved:

$$\min_{\Delta v_{fa},\, \Delta v_{f_b}, \Delta v_{f_b}} J \text{ s.t. (19) and (20)} \qquad J = a, b, c. \tag{21}$$

TABLE I
SYSTEM PARAMETERS IN GCOM

Parameters		Value
DG1–3	Inverter filter inductance	20mH
	Inverter filter resistance	0.1Ω
	DC-link voltage	520V
Grid voltage		230V
Reference values	ω_{ref}	314
	V_{ref}	230
Balanced load1 (S#1)	$R = 20\Omega, L = 6.5mH$	
	$R = 20\Omega, L = 6.5mH$	
	$R = 20\Omega, L = 6.5mH$	
Unbalanced load2 (S#2)	$R_1 = 15\Omega, L_1 = 10mH, R_2 = R_3 = 60.6\Omega$ $L_2 = L_3 = 30.3mH$	
Unbalanced load3 (S#2)	$R_1 = 10\Omega, L_1 = 10mH, R_2 = R_3 = 40\Omega,$ $L_2 = L_3 = 40mH$	

TABLE II
SYSTEM PARAMETERS IN IOM

Parameters	Value
V_{ref}	$230V$
ω_{ref}	$50Hz$
Load1	$R = 16\Omega, L = 16.5mH$
Load2	$R = 25\Omega$
Load3	$R = 25\Omega, L = 5mH$
Filter Inductance	$3mH$
Filter capacitance	$30\mu f$
DC-link voltage	$520Vdc$

C. MPC Design in IOM

Fig. 3 shows the schematic of the MPC for a three-phase inverter with an output LC filter in IOM. The output voltage $v_c[k]$, the filter current $i_f[k]$, inverter output voltage $v_i[k]$, and the DG output current $i_{\mathrm{DG}}[k]$ are measured and applied to calculate filter current and the output voltage at the subsequent sampling moment, i.e., $v_c[k+1]$ and $i_f[k+1]$, respectively, in (8). Using the predicted values at time step $k+1$, the output voltage and filter current at time step $k+2$ are predicted for the entire possible voltage vectors generated by the inverter (see Fig. 1). Utilizing the predicted values at time step $k+2$, the output voltage at time step $k+3$, i.e., $v_c[k+3]$, can be calculated. The cost function has been measured for seven possible predictions, and the voltage vector minimizes the function that has been chosen and used at time step $k+1$. Optimum switching mode

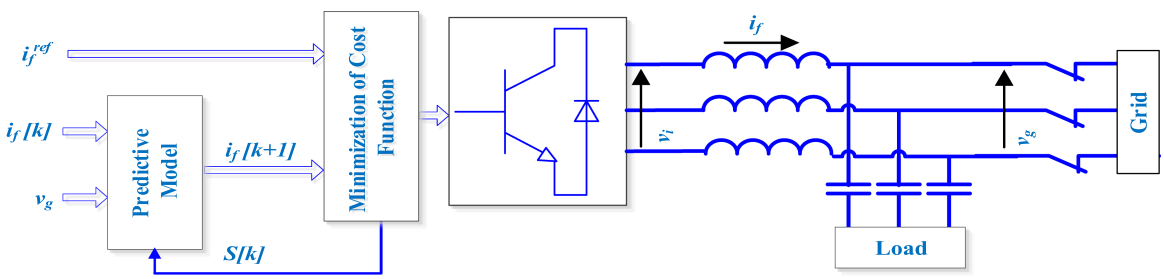

Fig. 4. Block schematic of MPC in GCOM.

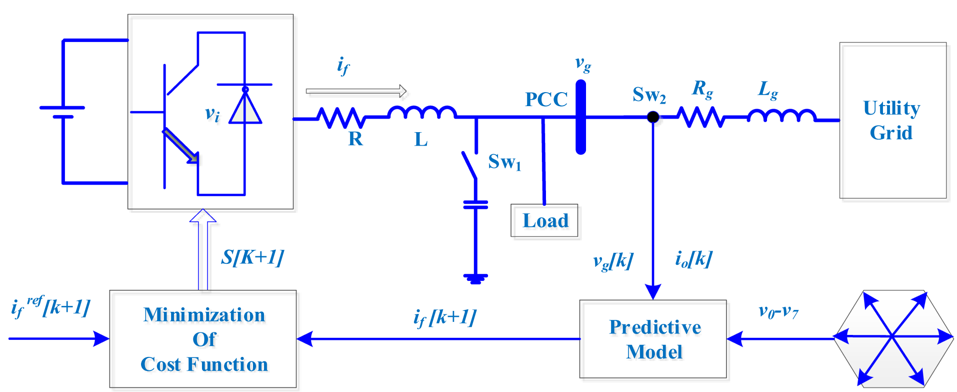

Fig. 5. Schematic diagram of the enhanced FCS-MPC.

minimizes the following cost function:

$$\text{Cos }t_{\text{IOM}} = \sum_{J=a,b,c} \left(v_c^J[k+3] - v_{\text{ref}}^J\right)^2 \tag{22}$$

where $v_c[k+3]$ describes as the capacitor voltage predicted at time step $k+3$ and v_{ref} gives the reference voltage. $a,\ b,$ and c denote the phases of a three-phase network.

D. MPC Design in GCOM

Fig.4 displays the schematic of the presented MPC for a three-phase inverter with an output L filter in GCOM. Grid voltage and filter current at time step k, i.e., $v_G[k]$ and $i_f[k]$, respectively, are calculated and applied to predict the filter current $i_f[k+1]$ using (8). This strategy uses seven possible voltage vectors produced through the inverter. Fig. 5 shows the schematic diagram of the enhanced FCS-MPC. The cost function has been evaluated for seven possible predictions, and the voltage vector that minimizes this function has been selected and used at step $k+1$. This cost function in GCOM is given as

$$\text{Cos }t_{\text{GCOM}} = \sum_{J=a,b,c} \left(i_f^J[k+1] - i_{f_{\text{ref}}}^J\right)^2 \tag{23}$$

where $i_f[k+1]$ describes as the inductor current predicted at time step $k+1$, $i_{f_{\text{ref}}}$ describes as a reference current, and $a,\ b,$ and c are the phases of a three-phase system.

E. Voltage Controller With Enhanced MPC

The main difference between the MG controller design and operation between IOM and GCOM is the voltage control. In the IOM, the inverters control the MG voltage, while in the GCOM, the MG voltage is controlled by the utility grid at the point of common coupling. The optimum switching state of the voltage controller and the voltage vector at time step k, i.e., $v_{cJn}^{\text{cal}}[k]$, is obtained through minimizing the following cost functions:

$$\text{Cos }t_{\text{Voltage}} = \left\| v_{cJn}^{\text{cal}}[k] - v_{cJn}^{\text{ref}}[k] \right\|,\ J = a, b, c. \tag{24}$$

Equation (24) is the closest state to the reference voltage vector at the time step , i.e., $v_{cJn}^{\text{ref}}[k]$. From (8), the predicted value of voltage $v_{cJn}[k]$ is calculated as $x_J^D[k] = A_D^{-1} x_J^D[k+1] - A_D^{-1} B_D v_i[k] - A_D^{-1}\Gamma_D i_o[k]$, and it can be written as follows:

$$\begin{aligned} v_{cJn}[k] &= m_1\, i_{f_{cJn}}[k+1] + m_2 v_g[k+1] + m_3 v_i[k] \\ &\quad + m_4 i_o[k] \\ i_{f_{cJn}}[k] &= m_5\, i_f[k+1] + m_6 v_g[k+1] \\ &\quad + m_7 v_i[k] + m_8 i_o[k] \\ J &= a, b, c. \end{aligned} \tag{25}$$

So, the selected voltage for the output voltage of a phase should be

$$\begin{aligned} v_{cJn}^{\text{cal}}[k] &= m_1\, i_{f_{\text{ref}}}^J[k+1] + m_2 v_{cJn}^{\text{ref}}[k+1] + m_3 v_i^J[k] \\ &\quad + m_4 i_{\text{load}_J}[k] \end{aligned}$$

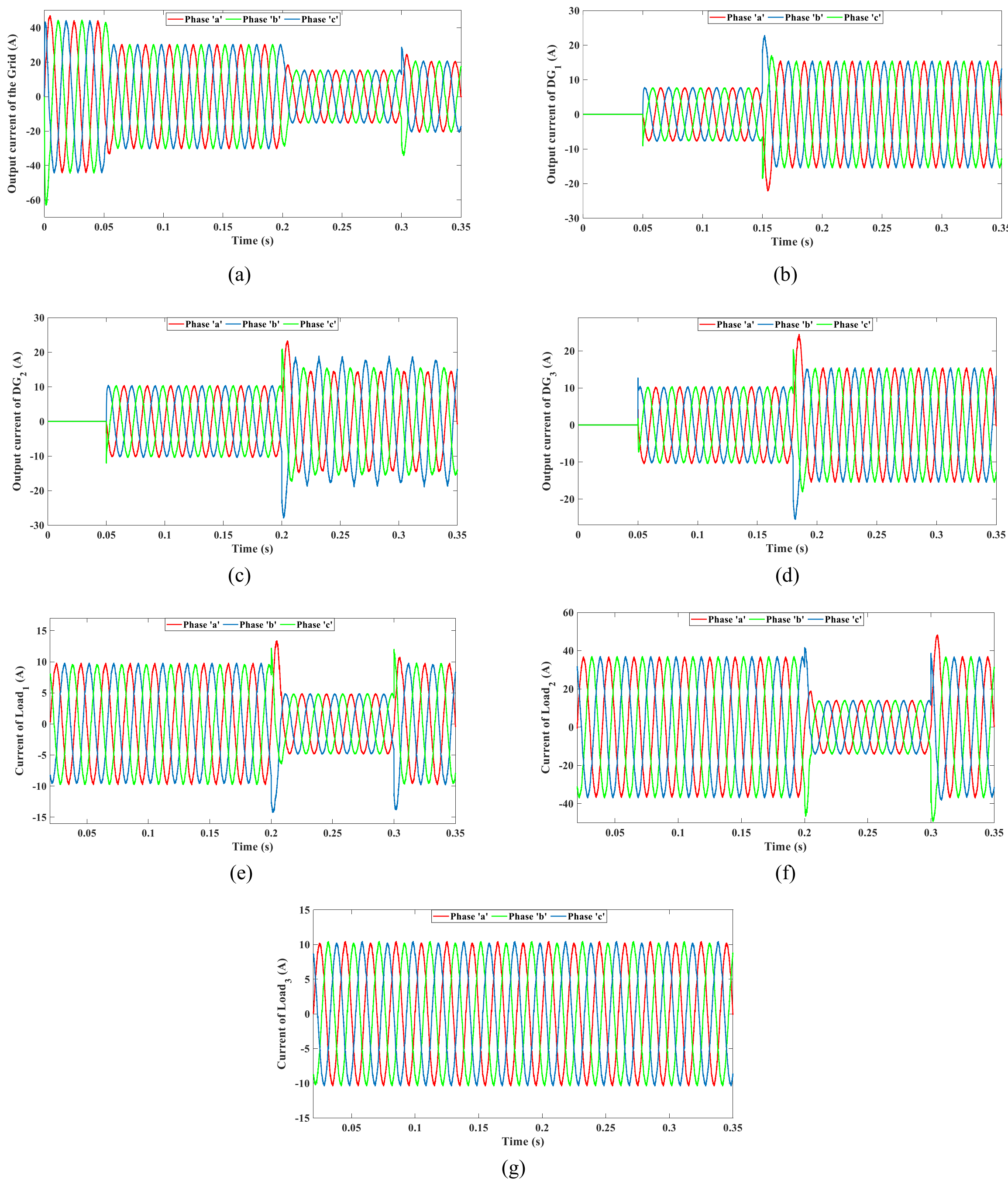

Fig. 6. (a)–(g) Output current waveforms of the utility, DG1, DG2, DG3, and loads currents in GCOM and S#1.

$$i_{f_{cJn}}^{\text{cal}}[k] = m_5\, i_{f_{\text{ref}}}^{J}[k+1] + m_6 v_{cJn}^{\text{ref}}[k+1] + m_7 v_i^{J}[k] + m_8 i_{\text{load}_J}[k]$$
$$J = a, b, c. \tag{26}$$

The control item, $v_i^J[k]$, is selected so that $v_{cJn}^{cJl}[k]$ in the abovementioned equation can minimize (24).

F. Power Flow Controller With Enhanced MPC

The power flow controller predicts the reactive and active powers and tries to set the switching state in one of eight possible switching states of (2) that minimizes the cost function. The cost function for the power flow controller is shown as follows:

$$\text{Cos}\, t_{\text{Power Flow}} = k_1 \left\| p_{\text{cal}}[k] - p_{\text{ref}}[k] \right\| + k_2 \left\| v_{\text{cal}}[k] - v_{\text{ref}}[k] \right\| \tag{27}$$

where $p_{\text{cal}}[k]$ and $p_{\text{ref}}[k]$ are the predicted three-phase active power and predicted three-phase reference active power at time step k, respectively, and $v_{\text{cal}}[k]$ and $v_{\text{ref}}[k]$ are the predicted three-phase voltage vector and three-phase reference voltage at time step $k+1$, respectively.

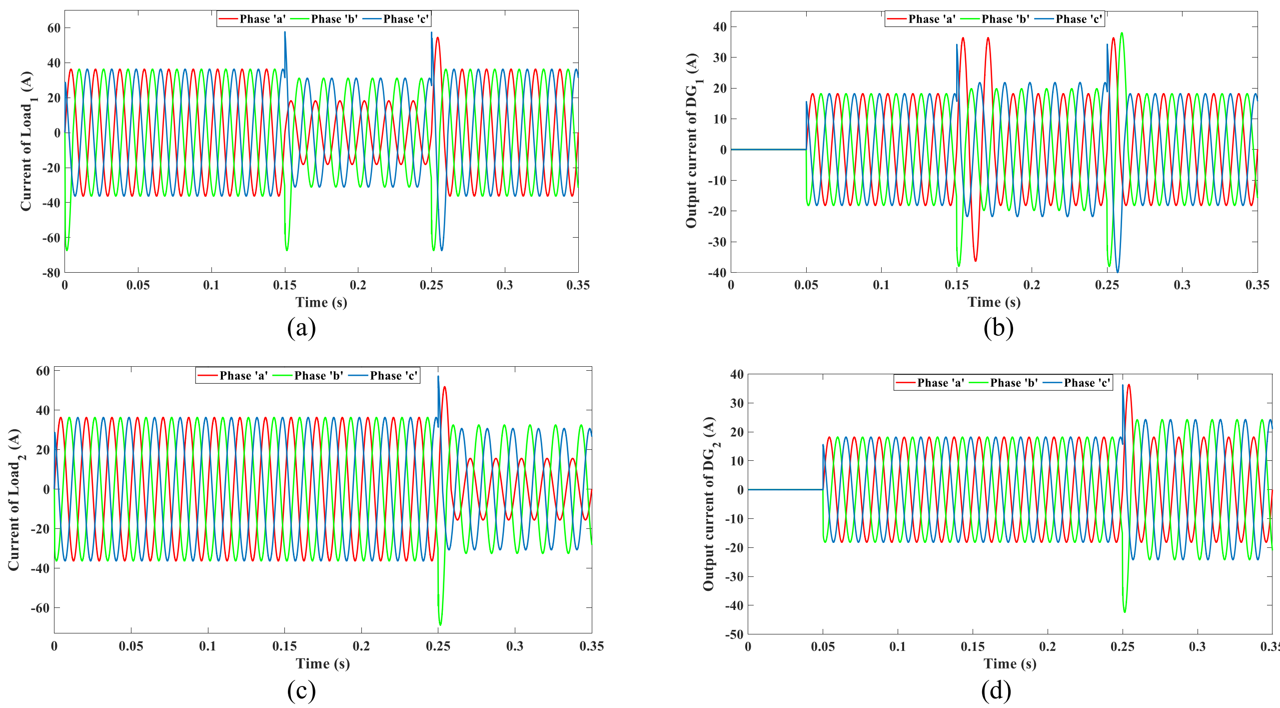

Fig. 7. (a)–(d) Output current waveforms of DG1 and DG2 and current waveforms of load1 and load2 in GCOM and S#2.

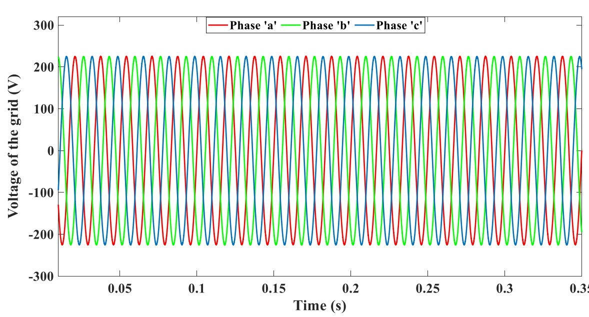

Fig. 8. Inverter output voltage of DG1 and DG2 after *L* filter in GCOM and S#2.

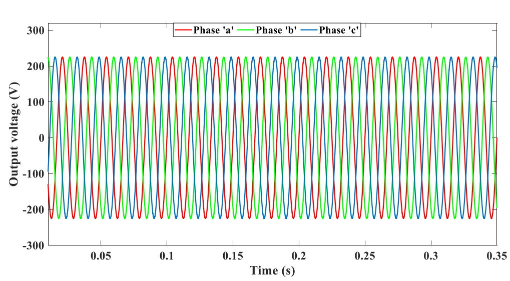

Fig. 9. Output voltage of DG in IOM.

In the power flow controller, it is required that $i^{J}_{f_{\text{ref}}}[k+1]$ and $v^{\text{ref}}_{cJn}[k+1]$ are followed. The control effort, $v_i[k]$, has to be found so that active power and output voltage track their references. The system parameters are presented in Tables I and II.

A. *Less Computation With Enhanced FCS-MPC*

The conventional FCS-MPC method selects the voltage vector v_n in such a way that the predicted current at time step $k+1$ and $i_f[k+1]$ can track the reference $i_f^{\text{ref}}[k+1]$ as close as possible. Based on (25), the current $i_f[k+1]$ would accurately follow the reference $i_f^{\text{ref}}[k+1]$, if the converter voltage operating at time instant k was controlled to follow the $v_{\text{can}}[k]$. The method includes eight times of calculating the current and minimizing the cost function in each stage. As can be seen from Fig. 5, it has restricted switching modes applied for the cost function. It reduces the current prediction at time step $k+1$ and to the solitary one time. The computational cost has been reduced to only once in determining the reference voltage and eight times in minimizing the cost function. The enhanced FCS-MPC applies the needed voltage vector ($v_{\text{can}}[k]$) for the prediction procedure. Since, in practical implementation, the maximum switching frequency is restricted, the advantage of decreasing the volume of computation is apparent.

IV. Simulation Results and Analysis

The effectiveness of the presented MPC approach for both GCOM and IOM is quantitatively evaluated in offline digital time-domain simulation using MATLAB software. The obtained simulation results are analyzed and compared with different control methods in the literature.

A. *GCOM (Power Quality Progression With Load Sharing)*

In the GCOM, DG units might supply reactive and active powers. The share of any DGs in providing the load was

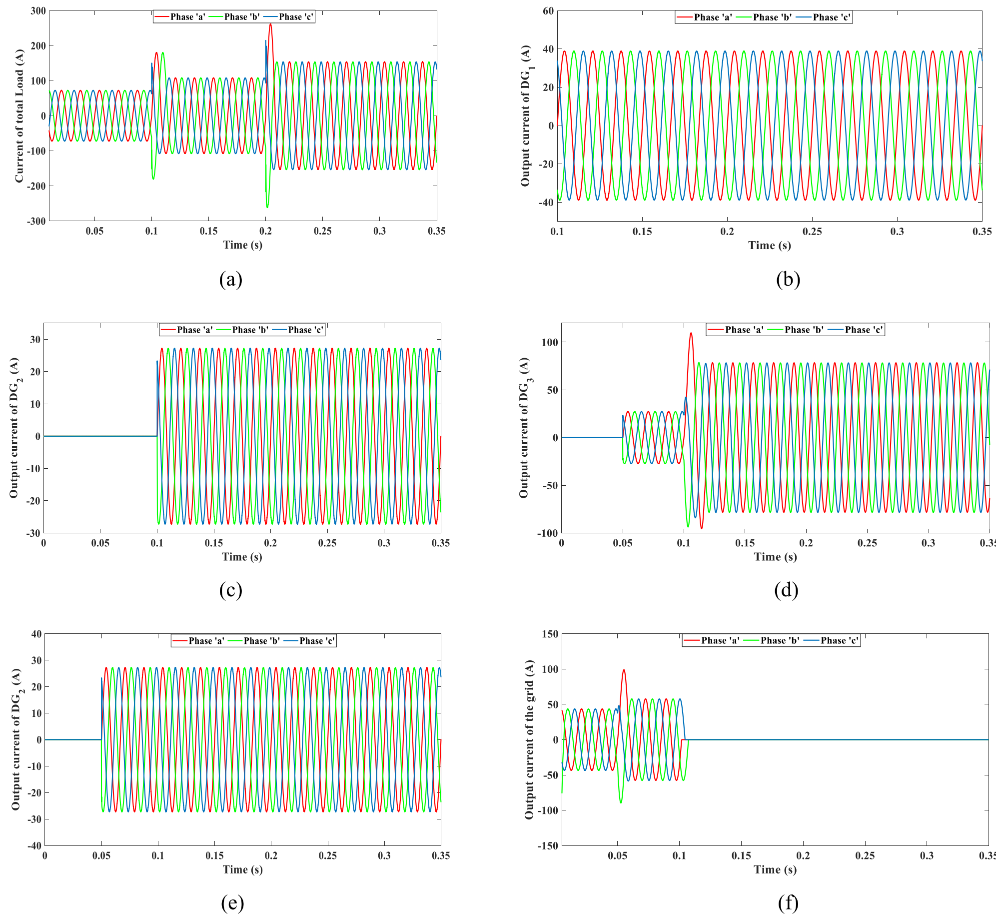

Fig. 10. (a)–(f) Output current of DG in IOM.

considered in the contribution factor (CF). DG operator or secondary controller determined CF based on optimization or practical considerations. In this simulation, the grid controlled MG's frequency and voltage. The connecting MG point to utility was practically treated as an infinite bus. The other points voltage was defined based on power flowing through lines, and the utility balanced the powers among load and DGs. The system was simulated based on the following assumptions.

1) The power flow between utility grid and MG is bidirectional. DGs can inject active power to the main grid in the peak hours and supply local loads.
2) Unbalanced loads can cause unbalanced voltages and currents in the network. In the existence of DGs, one or more DG units might cooperate to make up the unbalanced loads.

System parameters are given in Table I. The following two cases of unbalanced and balanced loads are considered in this case.

1) In the primary case (S#1), the load$_1$ is balanced; the total active and reactive loads were 19.7 kW and 4.8 kVAR, respectively. The load changes at $t = 0.\ 2$ s. Its active power alters 43%, and its reactive power varies by 58%. The load is increased as the same value at $t = 0.3$ s. All DGs are OFF at $t = 0$ s, and the grid supplied the load. The inverters are set ON with predefined setting values at $t = 0.05$ s. The active reference of DG-1 and DG-2 is altered at $t = 0.15$ and $t = 0.25$ s, respectively. The grid power changed at $t = 0.2$ s. However, DG-3 power stayed stable. The utility current signals, i.e., DG-1, DG-2, and DG-3, and loads for $t \in [\,0 \quad 0.35\,]$s are shown in Fig. 6.
2) The second scenario (S#2) in GCOM demonstrates that the proposed controller could effectively improve the power quality of the power utility when two DGs cooperated. At $t \in [\,0.15 \quad 0.25\,]s$, the unbalanced load$_1$ is joined to the DG-1 output. At $t \in [\,0.25 \quad 0.35\,]$s, the other unbalanced load$_2$ is joined to the DG-2 output. Each DG can compensate for its asymmetric power demand by generating more power. Fig. 7 shows the currents provided through DG-1 and DG-2, which have an unbalanced current to balance the utility current. The output voltage of DG2 and DG-1 after the L filter is equal to grid voltage, which is displayed in Fig. 8. The L filter is used to suppress the harmonics from the DG output current.

B. IOM (Load Sharing)

This scenario investigated the controller in IOM. At first, the grid was transferred to IOM from GCOM because of a fault in the grid at $t = 0.05$ s. The baseload for each DG was equal to load$_1$ (the details are mentioned in Table II). load$_2$ is added to the

TABLE III
QUANTITATIVE COMPARING THE PERFORMANCE OF MFCS-MPC WITH OTHER CONTROLLERS FOR PHASE "A"

Control method	Load	Fundamental (V)	Output voltage peak	Output voltage effective value	THD (%)	Third harmonic	Fifth harmonic	Maximum error	ISE=$\int e^2.dt$
MFCS-MPC	No load	220	222.21	157.14	0.29	0.13	0.31	2.21	0.45
	Symmetric load	220	222.12	157.08	0.32	0.20	0.27	2.12	0.50
	Non- symmetric load	220	221.8	156.86	0.43	0.21	0.31	1.8	0.54
	Nonlinear load	220	222.75	157.56	0.66	0.38	0.70	2.75	1.70
MPC	no load	220	217.35	153.71	0.72	0.37	0.41	2.65	0.62
	Symmetric load	220	216.72	153.26	0.70	0.41	0.48	3.28	0.76
	Non- symmetric load	220	215.65	152.53	0.99	0.36	0.38	4.35	0.60
	Nonlinear load	220	212.31	150.14	1.09	0.43	0.74	2.31	1.96
PID	no load	220	215.19	152.18	0.57	0.18	0.10	4.81	0.51
Control strategy (MPC-1) proposed in [33]	Symmetric load	311.12	306.9	-	2.09	-	-	4.22	-
	Non-symmetric load	311.12	300.5	-	5.08	-	-	10.62	-
	Nonlinear load	311.12	287.9	-	8.94	-	-	23.22	-
Control strategy (MPC-2) proposed in [33]	Symmetric load	311.12	309.4	-	1.10	-	-	1.72	-
	Non-symmetric load	311.12	307.8	-	1.55	-	-	3.32	-
	Nonlinear load	311.12	305.6	-	2.34	-	-	5.52	-
Control Method in [30]	-	200	198.4	138.88	2.74	3.546	1.885	1.6	-
Modified sliding mode controller with $\lambda = 5000$ [31]	-	110	107.2	75.8	0.88	0.55	0.09	2.8	-
Sliding mode controller with $\lambda = 5000$ [31]	-	110	105	74.27	1.05	0.36	0.23	5	-

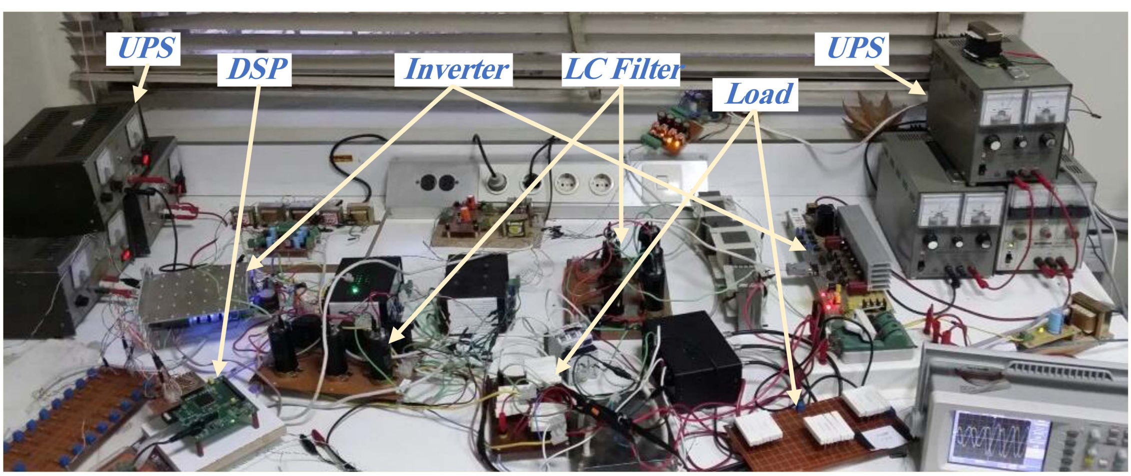

Fig. 11. Experimental laboratory setup.

grid local load at $t = 0.15$ s, and the load$_3$ is added at $t = 0.18$ s to the grid local load of DG1. load$_3$ is added to the local load of DG-2 and DG-3 at $t = 0.2$ and $t = 0.3$ s, respectively. Fig. 9 shows the output voltage of DG. The output current of DG is shown in Fig. 10.

In order to validate the proposed control scheme, an inverter connected to a changeable load is used for the experimental setup. Table III gives the specifications of the system. As can be seen from Table III, the proposed MFCS-MPC control technique improved the steady-state parameters, such as output voltage peak, output voltage effective value, and THD, compared to the other controllers, such as classic MPC, PI, FCS-MPC, FCS-MMPVC, sliding mode, and modified sliding mode [29], [30], [31], [32]. Also, compared to other control methods mentioned in [30], [31], and [32], the suggested strategy has a better performance in improving the steady-state parameters, such as output voltage peak, THD, integral square error (ISE), and also reduced maximum error.

V. EXPERIMENTAL STUDY

The proposed MPC method is also tested using hardware experiments. Fig. 11 shows the lab experimental test setup of the system. In the experimental test setup, we have two inverters controlled by the DSP TMSF28335 to confirm the efficiency of the presented theory and the simulation results. Here, the sampling frequency is equal to 10 kHz, the same as the switching frequency. Because the oscilloscope was a two-channel type, we

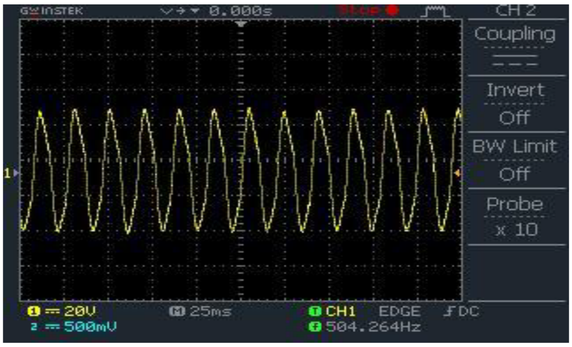

(a)

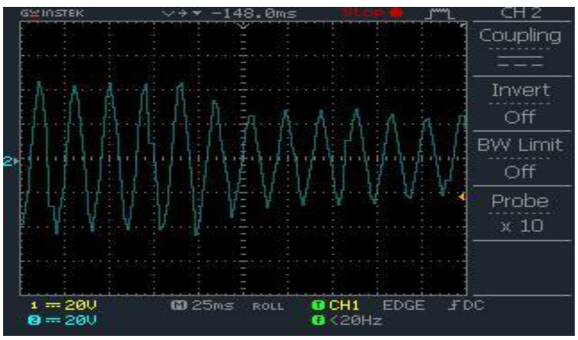

(b)

Fig. 12. Experimental results while the load is changed. (a) Output phase voltage "a". (b) Load current.

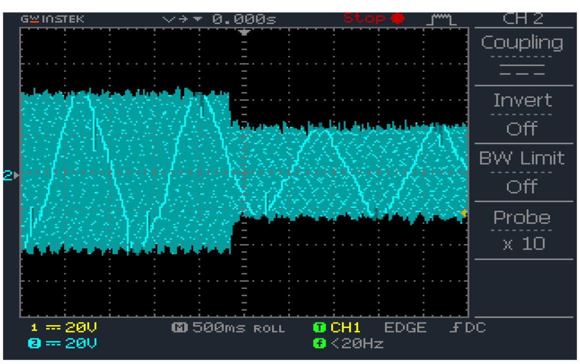

Fig. 13. Output voltage while a change in the value of reference voltage from 60 to 40 V is applied to the setup.

could only show a maximum of two signals in the results. Fig. 12 shows the load voltage [see Fig. 12(a)] while the load is changed [see Fig. 12(b)]. As shown in Fig. 12, as the load changed, the main voltage remained constant and the controller followed the reference signal well. Fig. 13 shows that the controller could effectively track the reference signal. For example, when the reference signal was reduced from 60 to 40 V, the controller followed the reference signal well. Fig. 14(a) shows the MG voltage and output current of unit-1, and Fig. 14(b) shows the output current of unit-2. As can be seen, the controller could follow the reference current signal well. Unit-2 supplied the entire load current. Also, the output current of unit-1 was almost zero, and unit-1 controlled the power well. The conventional FCS-MPC calculates the current eight times in each step, but the proposed FCS-MPC has been improved in this study, and only one time

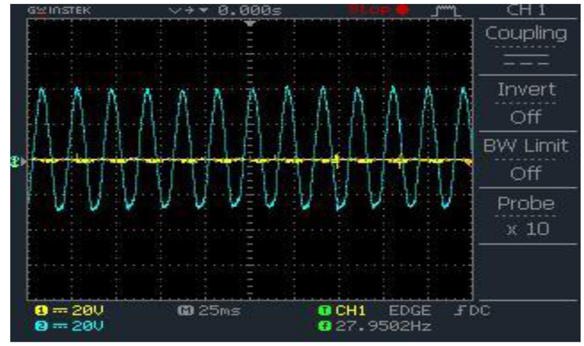

(a)

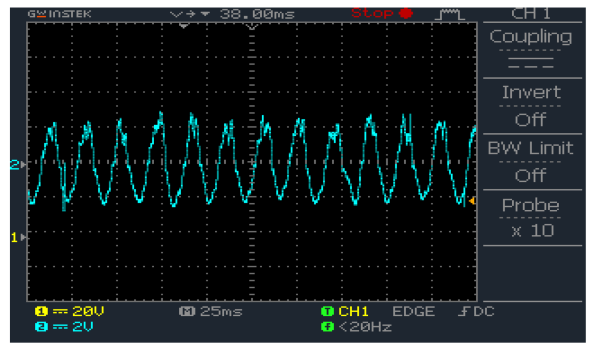

(b)

Fig. 14. Experimental result. (a) MG voltage and production current of the first DG. (b) Production current of the second DG.

is needed to calculate and specify the reference voltage. Hence, this is a significant improvement in practical implementation due to the maximum switching frequency limitation

VI. Conclusion

A novel multipurpose control scheme for renewable energy sources connected to the grid through converters in MGs was proposed in this research. The superiority of the proposed multipurpose control scheme was proved theoretically. The method involved a voltage control loop with the minimum inverter switching, a power-sharing control loop with the minimum inverter switching, a negative-sequence current controller, and a loop to identify the control system operation mode. All controllers were designed using MFCS-MPC.

These controllers can be used in GCOM and IOM and transferred between them by utilizing the dynamic inverter current and voltage. In IOM, the suggested voltage control loop maintains the MG bus voltage in an acceptable interval. For an unbalanced load, power components oscillate, and the negative-sequence current controller is applied to share the average power components of loads to separate the oscillating components. Each DG unit usually compensates for its local oscillating power. Oscillating power components of nonlocal loads are divided between whole DG units. Consequently, the suggested scheme decreases the negative-sequence current in the grid and dramatically improves the grid power quality.

In addition, the method applies voltage–frequency control instead of power control for inverters connected to a renewable energy source in both IOM and GCOM, especially under voltage in the weak grids. Considering one inverter as the voltage controller and others as the current controller may unstable the system in transient conditions. In response to this challenge, one inverter is selected as the main voltage controller and others control both current and voltage. Unlike other MPC methods, reactive and active powers are used, which are easily measured in the controller. The conventional FCS-MPC includes eight times calculating the current in each stage. Here, FCS-MPC is enhanced, and only one time computation is needed to determine the reference voltage. This is significant because the maximum switching frequency is limited in practical implementations. The outcomes of the simulation and practical implementations proved the advantage of the proposed control scheme. In future works, researchers can focus on designing practical and applicable control methods to enhance the transient stability of small-scale power systems. Also, it is suggested to design the same controller with observers and consider the system's performance under cyberattack conditions or design a robust controller that can highly guarantee the system's stability under cyberattacks in MGs. In this regard, the efficiency of the proposed method can be tested and analyzed under the delay of transmitted information from sensors or other agents.

REFERENCES

[1] A. Afshari, M. Karrari, H. R. Baghaee, G. B. Gharehpetian, and S. Karrari, "Cooperative fault-tolerant control of microgrids under switching communication topology," *IEEE Trans. Smart Grid,* vol. 11, no. 3, pp. 1866–1879, May 2020.

[2] C.-L. Chen, Y. Wang, J.-S. Lai, Y.-S. Lee, and D. Martin, "Design of parallel inverters for smooth mode transfer microgrid applications," *IEEE Trans. Power Electron.,* vol. 25, no. 1, pp. 6–15, Jan. 2010.

[3] M. Ghiasi, "Detailed study, multi-objective optimization, and design of an AC–DC smart microgrid with hybrid renewable energy resources," *Energy,* vol. 169, pp. 496–507, 2019.

[4] IEEE Std 1547™, *IEEE Standard for Interconnecting Distributed Resources with Electric Power Systems*, 2009.

[5] H. Jokar, B. Bahmani-Firouzi, and M. Simab, "Bilevel model for security-constrained and reliability transmission and distribution substation energy management considering large-scale energy storage and demand side management," *Energy Rep.*, vol. 8, pp. 2617–2629, 2022.

[6] M. B. Delghavi and A. Yazdani, "A control strategy for islanded operation of a distributed resource (DR) unit," in *Proc. IEEE Power Energy Soc. Gen. Meeting*, 2009, pp. 1–8.

[7] F. Katiraei, M. R. Iravani, and P. W. Lehn, "Micro-grid autonomous operation during and subsequent to islanding process," *IEEE Trans. Power Del.,* vol. 20, no. 1, pp. 248–257, Jan. 2005.

[8] M. Shafiee-Rad, M. S. Sadabadi, Q. Shafiee, and M. R. Jahed-Motlagh, "Robust performance satisfaction of DC microgrids using a decentralized optimal voltage control strategy," *IEEE Syst. J.,* vol. 16, no. 1. pp. 464–474, Mar. 2022.

[9] X. Tang, W. Deng, and Z. Qi, "Investigation of the dynamic stability of microgrid," *IEEE Trans. Power Syst.,* vol. 29, no. 2, pp. 698–706, Mar. 2014.

[10] D. Das, G. Gurrala, and U. J. Shenoy, "Linear quadratic regulator-based bumpless transfer in microgrids," *IEEE Trans. Smart Grid,* vol. 9, no. 1, pp. 416–425, Jan. 2018.

[11] H. Ueta and T. Yokoyama, "1MHz multisampling deadbeat control with disturbance compensation method for three phase PWM inverter," in *Proc. Int. Power Electron. Conf.*, 2018, pp. 1883–1889.

[12] M. S. Munsi, A. B. Siddique, S. K. Das, S. K. Paul, M. R. Islam, and M. A. Moni, "A novel blended state estimated adaptive controller for voltage and current control of microgrid against unknown noise," *IEEE Access,* vol. 7, pp. 161975–161995, 2019.

[13] H. Zhao, Q. Yang, and H. Zeng, "Multi-loop virtual synchronous generator control of inverter-based DGs under microgrid dynamics," *IET Gener., Transmiss. Distrib.,* vol. 11, pp. 795–803, 2017.

[14] M. Sitbon, I. Aharon, M. Averbukh, D. Baimel, and M. Sassonker, "Disturbance observer based robust voltage control of photovoltaic generator interfaced by current mode buck converter," *Energy Convers. Manage.*, vol. 209, 2020, Art. no. 112622.

[15] P. Cortes, G. Ortiz, J. I. Yuz, J. Rodriguez, S. Vazquez, and L. G. Franquelo, "Model predictive control of an inverter with output *LC* filter for UPS applications," *IEEE Trans. Ind. Electron.*, vol. 56, no. 6, pp. 1875–1883, Jun. 2009.

[16] M. Jafari, Z. Malekjamshidi, and J. Zhu, "A magnetically coupled multi-port, multi-operation-mode micro-grid with a predictive dynamic programming-based energy management for residential applications," *Int. J. Elect. Power Energy Syst.,* vol. 104, pp. 784–796, 2019.

[17] P. Ponnambalam, M. Praveenkumar, J. B. Edward, J. G. Shankar, G. Gokulakrishnan, and K. Aroul, "Comparison of fuzzy and MPC based flying capacitor multicell inverter," in *Proc. IEEE Region 10 Conf.*, 2016, pp. 70–76.

[18] E. Z. Bighash, S. M. Sadeghzadeh, E. Ebrahimzadeh, and F. Blaabjerg, "High quality model predictive control for single phase grid-connected photovoltaic inverters," *Electric Power Syst. Res.*, vol. 158, pp. 115–125, 2018.

[19] B. Mayer, M. Killian, and M. Kozek, "Management of hybrid energy supply systems in buildings using mixed-integer model predictive control," *Energy Convers. Manage.*, vol. 98, pp. 470–483, 2015.

[20] M. Ma, H. Chen, X. Liu, and F. Allgöwer, "Distributed model predictive load frequency control of multi-area interconnected power system," *Int. J. Elect. Power Energy Syst.*, vol. 62, pp. 289–298, 2014.

[21] S. Mariéthoz and M. Morari, "Explicit model-predictive control of a PWM inverter with an *LCL* filter," *IEEE Trans. Ind. Electron.*, vol. 56, no. 2, pp. 389–399, Feb. 2009.

[22] M. Novak, U. M. Nyman, T. Dragicevic, and F. Blaabjerg, "Statistical model checking for finite-set model predictive control converters: A tutorial on modeling and performance verification," *IEEE Ind. Electron. Mag.*, vol. 13, no. 3, pp. 6–15, Sep. 2019.

[23] J. Hu, Y. Li, and J. Zhu, "Multi-objective model predictive control of doubly-fed induction generators for wind energy conversion," *IET Gener., Transmiss. Distrib.,* vol. 13, pp. 21–29, 2019.

[24] T. Geyer, "A comparison of control and modulation schemes for medium-voltage drives: Emerging predictive control concepts versus PWM-based schemes," *IEEE Trans. Ind. Appl.,* vol. 47, no. 3, pp. 1380–1389, May/Jun. 2011.

[25] M. Preindl, E. Schaltz, and P. Thogersen, "Switching frequency reduction using model predictive direct current control for high-power voltage source inverters," *IEEE Trans. Ind. Electron.*, vol. 58, no. 7, pp. 2826–2835, Jul. 2011.

[26] K. H. Ahmed, A. M. Massoud, S. J. Finney, and B. W. Williams, "A modified stationary reference frame-based predictive current control with zero steady-state error for *LCL* coupled inverter-based distributed generation systems," *IEEE Trans. Ind. Electron.,* vol. 58, no. 4, pp. 1359–1370, Apr. 2011.

[27] Y. Zhang, Z. Wang, J. Jiao, and J. Liu, "Grid-voltage sensorless model predictive control of three-phase PWM rectifier under unbalanced and distorted grid voltages," *IEEE Trans. Power Electron.*, vol. 35, no. 8, pp. 8663–8672, Aug. 2020.

[28] K. Zaouche, S. M. Benmerabet, A. Talha, and E. M. Berkouk, "Finite-set model predictive control of an asymmetric cascaded H-bridge photovoltaic inverter," *Appl. Surf. Sci.*, vol. 474, pp. 102–110, 2019.

[29] S. Golzari, F. Rashidi, and H. F. Farahani, "A Lyapunov function based model predictive control for three phase grid connected photovoltaic converters," *Sol. Energy,* vol. 181, pp. 222–233, 2019.

[30] T. Jin, X. Shen, T. Su, and R. C. C. Flesch, "Model predictive voltage control based on finite control set with computation time delay compensation for PV systems," *IEEE Trans. Energy Convers.,* vol. 34, no. 1, pp. 330–338, Mar. 2019.

[31] Y. Hinago and H. Koizumi, "A single-phase multilevel inverter using switched series/parallel DC voltage sources," *IEEE Trans. Ind. Electron.,* vol. 57, no. 8, pp. 2643–2650, Aug. 2010.

[32] M. Dehghani, M. H. Khooban, T. Niknam, and S. Rafiei, "Time-varying sliding mode control strategy for multibus low-voltage microgrids with parallel connected renewable power sources in islanding mode," *J. Energy Eng.,* vol. 142, 2016, Art. no. 05016002.

[33] E. Hossain, J. Hossain, and F. Un-Noor, "Utility grid: Present challenges and their potential solutions," *IEEE Access,* vol. 6, pp. 60294–60317, 2018.